SAND99-3147J

Residual Stress Predictions in Polycrystalline Alumina

Venkata R. Vedula[1], S. Jill Glass[1], David M. Saylor[2], Gregory S. Rohrer[2], W. Craig Carter[3], and Stephen A. Langer[4]

[1] Ceramic Materials Department, Sandia National Laboratories, Albuquerque, NM 87185
[2] Department of Materials Science and Engineering, Carnegie Mellon University, Pittsburgh, PA 15213
[3] Department of Materials Science and Engineering, Massachusetts Institute of Technology, Cambridge, MA 02139
[4] Mathematical and Computational Sciences Division, National Institute of Standards and Technology, Gaithersburg, MD 20899

Abstract

Microstructure-level residual stresses arise in polycrystalline ceramics during processing as a result of thermal expansion anisotropy and crystallographic misorientation across the grain boundaries. Depending upon the grain size, the magnitude of these stresses can be sufficiently high to cause spontaneous microcracking during the processing of these materials. They are also likely to affect where cracks initiate and propagate under macroscopic loading.

The magnitudes of residual stresses in untextured and textured alumina samples were predicted using object oriented finite (OOF) element analysis and experimentally determined grain orientations. The crystallographic orientations were obtained by electron-backscattered diffraction (EBSD). The residual stresses were lower and the stress distributions were narrower in the textured samples compared to those in the untextured samples. Crack initiation and propagation were also simulated using the Griffith fracture criterion. The grain boundary to surface energy ratios required for computations were estimated using AFM groove measurements.

DISCLAIMER

DISCLAIMER

Portions of this document may be illegible in electronic image products. Images are produced from the best available original document.

1. Introduction

Residual stresses arise in polycrystalline ceramics during processing as a result of thermal expansion anisotropy and crystallographic misorientation across the grain boundaries. During microstructural evolution, boundaries with higher mobilities and energies are likely to be eliminated, thereby changing the distribution of lattice orientations and misorientations. This process is expected to change the distribution of grain orientations (and misorientations) with increasing grain size to one that is less random. The magnitude and distribution of stresses therefore are likely to depend on the grain size and degree of texture in the samples.

When a polycrystalline material with non-cubic crystal symmetry is subject to a temperature change, each grain will attempt to strain differently than its neighbors, resulting in residual stresses and strains in the material. In brittle materials, the thermal strains that result during cooling from the sintering temperature can be comparable to the fracture strain of the material leading to internal cracking, also known as spontaneous microcracking. The onset of microcracking depends on the grain (crystal) size and below a critical value, no spontaneous microcracking occurs. The stresses generated in a material do not depend on the grain size, however, the strain energy does. Assuming that enough stress and potential microcrack formation sites are available, it has been shown that the formation of microcracks in ceramics is governed by the stored elastic strain energy.[1] A microstructural model proposed by Sridhar et al.[2] showed that although large grain sizes are more detrimental with regard to their fracture properties, the total length or area of all cracks in a sample is larger when grain size is small. Therefore, the decrease in elastic modulus will be larger in small grain samples.[2]

Highly textured microstructures have been shown to drastically reduce the residual stresses associated with thermal contraction anisotropy in alumina.[3] Moreover, it was found that the crack propagation is also inhibited in the through-thickness direction. More recently, it has also been shown that under multiple Hertzian indentation loadings, the damage evolution rate is much lower for the textured samples.[4] In addition to grain size and texture in samples, grain shape distribution and the extent to which stress relaxation mechanisms are active will also influence the variation of residual stresses. However, for the purposes of this paper, it will be assumed that no stress relaxation mechanisms are active.

Residual stresses are critical to the R-curve behavior that occurs in ceramics. In ceramic containing components, macroscopic residual stresses arise due to thermal expansion mismatch between different materials.[5] The interaction between macro- and microscopic residual stresses can significantly influence the crack initiation and propagation in the ceramic and affect the component reliability.

This paper presents a methodology to predict residual stresses in ceramics using experimentally determined grain orientations in conjunction with object oriented finite (OOF) element analysis. The critical temperature for microcrack formation in alumina was also predicted as a function of grain size. Crystallographic orientations and relative grain boundary energies required for predictions were obtained using electron backscattered diffraction (EBSD) and atomic force

microscopy (AFM) respectively. The magnitude of stresses and stress distributions in untextured and textured alumina are compared.

2. Experimental Details

(a) Materials Studied

The untextured samples used in this study were prepared from 99.99% pure alumina powder (AKP-50, Sumitomo Chemical America, New York, NY). The powder was compacted in a uniaxial press at 28 MPa and then isostatically pressed at 280 MPa. The pressed pellets were packed in a crucible with the parent powder and fired at 1600°C for 5 hrs. Details of processing can be found elsewhere.[6] The average grain size of the samples was 10 and 27 μm. The samples were ground flat and polished by diamond paste. The final polishing step used colloidal silica (pH=10). Textured alumina samples were prepared by gel casting. Samples were prepared by lay-up of tapes containing aligned alumina platelets. The final microstructure had non-equiaxed, plate like grains and a very strong preferred orientation with the c-axis perpendicular to the plane of the tapes.[7]

(b) EBSD measurements

The orientations of individual grains on the surface of samples were obtained using electron backscattered diffraction (EBSD). The technique involves use of an electron beam incident on a sample titled at 70° to the beam normal. The interaction of the electron beam with the sample generates a diffraction cone that can be recorded on a phosphor screen. The patterns (known as Kikuchi diffraction patterns) can be indexed to determine the orientation of that grain with reference to a reference axis. The patterns were collected using a scanning electron microscope (Phillips SL40FEG). Scans were performed in a hexagonal grid with a spacing of 3 and 1.5 μm in untextured and textured samples respectively. The grid of measured orientations defines the position and size of each grain. A commercially available system, Orientation Imaging Microscopy® (OIM) was used to automatically collect and index the patterns (TSL, Inc., Draper, UT). The technique allows a large number of grains to be characterized in a single scan.

(c) AFM groove measurements

The width and depth of the thermal grooves formed by the grain boundaries were measured by atomic force microscopy (AFM) to determine the ratio of the grain boundary free energy (γ_{gb}) to the surface free energy (γ_s).[8] Dihedral angles were measured using a StandAlone AFM (#SAA-125, Digital Instruments, Tonawanda, NY) positioned above the sample mounted on a X-Y translation stage (Burleigh Instruments, #TSE-150, Fishers, NY) with reproducible position resolution of 50 nm. Readers are referred to Ref. 8 for details on imaging and error minimization. The samples were thermal grooved at 1600°C for 100 hours. The ratio γ_{gb}/γ_s was obtained using the simplified Herring equation: $\gamma_{gb}/\gamma_s=2\cos(\psi/2)$ where ψ is the surface dihedral angle. This equation assumes that the torque terms are zero, the surface energies are isotropic, and the grain boundary energy is a function of misorientation alone and not of the boundary plane inclination.

3. Finite Element Analysis

(a) Object oriented finite (OOF) element analysis

OOF is an object oriented finite element analysis code developed at NIST.[9] It is designed to investigate the response of microstructures to mechanical and thermal loads. The program performs thermoelastic calculations in two dimensions (plane strain or plane stress) using 3-node triangular elements. Several "smart" meshing schemes based on energy minimization are available to mesh curved features, such as grain boundaries. A digital image of a microstructure, either from an optical/electron microscope or a result of a computer simulation can be used for analysis. The user specifies crystallographic orientations, elastic, and thermal properties for the various regions (grains) in the microstructure. Based on this information, a finite element grid with associated properties is generated on which mechanical and/or thermal loading can be applied. A solution is then obtained for the specified boundary conditions, distortion, and temperature change.

(b) OIM-2-OOF code

The methodology of manually assigning properties to various grains in a microstructure works well when working with smaller microstructures (≈100 grains). The objective of this work was to analyze stresses and stress distributions in large microstructures to gather statistically reliable data. A code (OIM-2-OOF) was therefore developed that allows crystallographic orientations from Orientation Imaging Microscopy® (OIM) to be directly imported into OOF. An OIM scan is typically done in a hexagonal grid, as shown in **Fig. 1**. The user species the step size and the x- and y-axes ranges for the scan. The OIM-2-OOF code converts the data from the hexagonal grid to a square grid, generates an image, and writes an intermediate file that contains information regarding the grains and their respective crystallographic orientations. This code allows the user to analyze residual stress distributions in large microstructures (>600 grains) with relative ease. The code also detects grain boundaries and assigns respective relative grain boundary energies (obtained by groove measurements) automatically.

(c) Crack propagation in ceramics

The elements in OOF code are designed to fail under the Griffith criterion, which states that a crack will propagate when the total surface energy required to propagate the crack can be supplied by the elastic energy stored in the body;

$$2l\gamma < \tfrac{1}{2}\int \sigma\varepsilon dV \qquad (1)$$

where l is the crack length and γ is the surface energy of the cracked interface. The element size is used to specify the characteristic crack length and the volume of integration is the element area (per unit depth).

The analysis involves the following steps:

(a) Thermal and mechanical loads are applied and the microstructure is equilibrated to determine stress/strain distribution.
(b) The energy balance is computed.
(c) If an element reaches the critical energy density (i.e., favorable for cracking), the direction of the principal stress axis is determined. The

stiffness matrix is rotated into a new coordinate system in which the principal stress lies along the z axis. In the rotated coordinate system, Czzzz and all other components of Cijkl with at least one of ijkl=z are multiplied by 0. The stiffness matrix is rotated back into its original orientation. The stiffness of the element is therefore reduced anisotropically to simulate a crack.

(d) The microstructure is re-equilibrated and the stress distribution is re-calculated.

(e) The procedure is repeated until no more elements mutate or one or more cracks become unstable causing fracture into two or more fragments.

4. Results and Discussion

(a) Residual stress distributions in untextured and textured alumina

Residual stresses in alumina (>650 grains) due to its thermal expansion anisotropy were estimated using the OIM-2-OOF and OOF codes. The orientations of grains, elastic, and thermal properties were input into OOF to predict the residual stresses. The orientations obtained by EBSD were input as a set of Euler angles (α, β, γ). The orientation map of the microstructure is shown in **Fig. 2(a)**. The grains are color-coded, where each color represents an orientation normal to the specimen surface, as shown by the stereographic triangle. It is clear that there is no macroscopic texture in this sample. The pole figures from EBSD data showed MRD (multiples of random distribution) value of 2. The OOF simulation used 117612 elements. The elastic stiffness constants and coefficients of thermal expansion for α-alumina (trigonal crystal symmetry) used in the analysis were C_{11}=497 GPa, C_{12}=163 GPa, C_{13}=111 GPa, C_{14}= -23.5 GPa, C_{33}=498 GPa, C_{44}=147 GPa, α_{11}=8.6x10^{-6} /°C, and α_{33}=9.3x10^{-6} /°C.[10] The calculations were done assuming plane stress and free boundary conditions to mimic unconstrained cooling of a thin plate from its sintering temperature. **Fig. 2** shows the microstructure (OIM output), stress invariant 1 (σ_{11} + σ_{22}), and maximum principal stress distributions for a temperature change of -1500°C. The highest value of the maximum principal stress was fairly high (≈530 MPa). The highest stresses were localized at the grain boundaries and triple junctions and drop rapidly away from the boundaries (**Fig. 3**). The maximum principal stress was comparable to typical fracture strength of this material. The residual stress distributions were almost identical in the 10 and 27 μm samples indicating no or negligible effect of grain size (orientations were random in both cases). The stresses within the grains (≈100-200 MPa) compare favorably with those measured by spectroscopic[11] and fluorescence imaging[12]. There appear to be regions of tensile and compressive stress on a scale that is larger than the grain size (**Fig. 2c**). Analysis is continuing to understand this observation.

Residual stresses were also predicted for textured alumina. The sample was textured in c-axis with MRD (multiples of random distribution) value of 90. The number of grains and the total number of elements (=117612) were same as that used for analyzing untextured sample. As one would expect, the stresses were much smaller in this sample compared to "randomly-oriented" samples. The largest

maximum principal stress was ≈ 415 MPa. **Fig. 4** shows the microstructure, stress invariant 1, and the maximum principal stress for a temperature change of -1500°C. The number of elements versus their stress value (stress invariant 1) is plotted for both textured and untextured sample in **Fig. 5**. The number of elements with high stresses is much lower in the textured sample than in the untextured sample. In both cases, the number of elements with high stresses is very small. In the untextured sample, <5% of the total elements had high stresses (>250 and <-250 MPa). The corresponding number in the textured sample was <0.4%.

Stress predictions were also made on periodic equiaxed microstructures generated by the Pott's model[13] to validate the boundary conditions. The residual stresses in the original microstructure and one with a periodicity of 3x3 (9 times the original image) were compared using free boundary conditions. The stresses and stress distributions obtained in both cases were almost identical indicating that stress predictions are true and free boundary conditions (free edges) do not lead to any artificial effects. It should be noted that the stress calculations are purely elastic and assume no stress relaxation mechanisms are active. In reality, diffusional flow, plastic deformation, and microcracking will relax the constraints between the grains and reduce the residual stresses.

(b) Crack initiation and propagation

In ceramics, cooling from the sintering temperature (≈1550°C for alumina) can create sufficiently high stresses to cause microcracking. The effect of grain size on the critical temperature for microcracking in alumina was determined using the microstructure in **Fig. 6** by varying the dimensions of the image, i.e., different length scales were used to represent different grain sizes.

The energy required for crack propagation through a grain is $2\gamma_s$ and through a grain boundary (intergranular) is $2\gamma_{ig}=(2\gamma_s - \gamma_{gb})$, where γ_s is the surface energy of grains and γ_{gb} is the grain boundary energy. γ_{gb}/γ_s values were obtained from AFM groove measurements. The surface energy of grains (γ_s) was taken as 2 J/m^2 and that of individual boundaries was calculated using $\gamma_{ig}=(4 - \gamma_{gb})/2$. γ_{ig} varied between 0.59 and 1.17 J/m^2. The grain boundary elements were assigned the elastic properties of glass (isotropic crystal symmetry), E=70 GPa and ν=0.23. The elements in the model representing grains were assigned a surface energy of 2 J/m^2 and the boundary elements were assigned their respective γ_{ig} values. The surface energy anisotropy in alumina has been reported at approximately 12%.[14] However, in the present analysis the surface energy of alumina is assumed isotropic.

The properties of the grain boundary glass phase are expected to influence the stress distribution and critical temperature for microcracking. Two different glass compositions were considered for grain boundary phase, namely, a high CaO and a high MgO glass. A high CaO glass has $\alpha \approx 9.5\text{x}10^{-6}$ /°C, which results in tensile residual stresses at grain boundaries, whereas for a high MgO glass ($\alpha \approx 5\text{x}10^{-6}$ /°C), compressive stresses result at the grain boundaries.[15] These compositions and associated properties were chosen as they represent the bounds on the type of grain boundary glass phase typically found in alumina.

Microcrack propagation was simulated with increasing temperature difference using the procedure described in 3(c). **Fig. 6** shows initiation of microcracks at the

triple junctions when ΔT=-925 to -1500°C. It has been shown numerically that the largest stress intensification occurs at the triple junctions.[16] With increasing temperature difference (thermal strain), microcracks initiated at new sites and coalescence of microcracks was also observed to form large cracks. As can be seen, damage occurred at several regions and some of the boundaries were completely cracked.

The expected inverse square root grain size relationship to increasing temperature[17] was found, as shown in **Fig. 7**. The critical grain size for microcracking for an alumina sample cooled from a 1600°C sintering temperature with high CaO glass grain boundary phase was 238 μm and with high MgO phase was 47 μm. Calculations were also made for case where there is no glass present at the grain boundaries. The boundary elements on either side of the interface were assigned the properties of alumina and the respective grain orientations. The surface energy of elements was that determined by AFM groove measurements. In this case the critical grain size was found to be 351 μm. Experimentally, critical grain size values have been reported between 40-200 μm.[18] It should be noted that plane stress conditions underestimate the residual stress values, hence in reality, the critical grain size values are expected to be lower.

(c) Effect of grain boundary thickness

In the crack propagation analysis above, it was assumed that when glass phase is present, all grain boundaries are wet and the boundary thickness is constant (≈1 μm). It has been shown that wetting of interfaces and thickness of boundaries is far more complicated. The wetting behavior depends on the crystal misalignment and interface orientation[19] and the thickness of grain boundary phase, when it exists, is of the order of 1-10 nm.[20] Three-dimensional Wulff constructions have shown that transitions from dry to partially wetted to fully wetted boundary depend on the grain boundary misorientation, grain boundary plane orientation, and the energies of grain boundary and the wetted interface.[21] The initial separation between crystalline particles is also likely to play a role in the presence and thickness of grain boundary films.[22]

Due to computational limitations, it was not possible to consider the grain boundary thickness of less than 0.5 μm in the analysis. A set of calculations was done on a smaller microstructure to determine the effect of the boundary thickness on residual stresses and critical temperature for microcracking (**Fig. 8**). The thickness of the boundary was varied from 20 to 140 nm. The mesh size and the number of elements (=379904) were kept constant in the calculations. **Table 1** shows the effect of thickness on stress values. As the thickness decreases, the stresses increase, which is intuitive as the constraint on the grain boundary from neighboring grains increases. **Fig. 9** shows that the critical temperature for cracking is also strongly dependent on the grain boundary thickness. With increase in thickness, the critical temperature increases. This is related to the changes in the stress and strain energy density. It should be noted that the effects of stress relaxation and grain boundary thickness are inverse of each other. Therefore, the use of artificially thicker grain boundary compensates at least partly for the stress relaxation effects not accounted for in the analysis.

5. Conclusions

This study is the first in predicting residual stresses in alumina using measured experimental grain orientations. The magnitudes of residual stresses in untextured and textured alumina were predicted using object oriented finite element analysis and experimentally determined orientations. The stresses were found to be very high and localized at the grain boundaries. The residual stresses were lower and the stress distributions were narrower in textured samples compared to those in untextured samples. Microcrack initiation and propagation were simulated using the Griffith criterion and measured grain boundary energies. The increase in damage with increasing temperature difference occurred by both formation of new cracks and propagation of existing cracks. It is important to note that besides stresses, other factors that determine the onset of microcracking include the size and location of existing flaws as these can act as nucleation sites for microcracks.

Acknowledgements

Sandia is a multiprogram laboratory operated by Sandia Corporation, a Lockheed Martin Company, for the United States Department of Energy under Contract DE-ACO4-94AL85000.

The authors would like to acknowledge Profs. David Brandon and Desiderio Kovar for the samples used in this study. The work performed at CMU was supported in part by the MRSEC Program of the National Science Foundation under Award Number DMR-9632556.

References

[1] J. A. Kuszyk, and R. C. Bradt, "Influence of Grain Size on Effects of Thermal Expansion Anisotropy in $MgTi_2O_5$", *J. Am. Ceram. Soc.*, **56**[8] 420-3 (1973).
[2] N. Sridhar, W. Yang, D. J. Srolovitz, and E. R. Fuller, "Microstructural Mechanics Model of Anisotropic Thermal Expansion Induced Microcracking", *J. Am. Ceram. Soc.*, **77**[5] 1123-38 (1994).
[3] T. Carisey, I. Levin, and D. G. Brandon, "Microstructure and Mechanical Properties of Textured Al_2O_3", *J. Euro. Ceram. Soc.*, **15**[4] 283-9 (1995).
[4] L. An, "Indentation Fatigue in Random and Textured Alumina Composites", *J. Am. Ceram. Soc.*, **82**[1] 178-82 (1999).
[5] V. R. Vedula, S. J. Glass, S. L. Monroe, and C. Newton, "Reliability and Lifetime Predictions for Ceramic Components", 23rd Annual Cocoa Beach Conference, Cocoa Beach, FL, 1999, In press.
[6] D. Kovar, "The Role of Microstructure on the Mechanical Reliability of Alumina Ceramics", Ph.D. Thesis, Carnegie Mellon University, Pittsburgh, PA (1995).
[7] T. Carisey, A. Laugier-Werth, and D. G. Brandon, "Control of Texture in Al_2O_3 by Gel-casting", *J. Euro. Ceram. Soc.*, **15** 1-8 (1995).
[8] D. M. Saylor and G. S. Rohrer, "Measuring the Influence of Grain-Boundary Misorientation on Thermal Groove Geometry in Ceramic Polycrystals", *J. Am. Ceram. Soc.*, **82**[6] 1529-36 (1999).
[9] OOF version 1.0.7, Center for Theoretical and Computational Materials Science (CTCMS), *National Institute of Standards and Technology (NIST)*, Gaithersburg, MD (1999).
[10] J. B. Wachtman, W. E. Tefft, D. G. Lam, R. P. Stinchfield, "Elastic Constants of Synthetic Single Crystal Corundum at Room Temperature", *J. Res. Nat. Bur. Std.*, **64A** 213-28 (1960).

[11] Q. Ma and D. R. Clarke "Piezospectroscopic Determination of Residual Stresses in Polycrystalline Alumina", *J. Am. Ceram. Soc.*, 77[2], 298-302 (1994).
[12] R. H. Dauskardt and J. W. Ager, "Quantitative Stress Mapping in Alumina Composites by Optical Fluorescence Imaging", *Acta. Mater.*, 44[2] 625-41 (1996).
[13] D. J. Srolovitz, M. P. Anderson, G. S. Grest, and P. S. Sahni, "Grain Growth in Two-dimension", *Scr. Metall.*, **17**, 241-46 (1983).
[14] J.-H. Choi, D.-Y. Kim, B. J. Hockey, S. M. Wiederhorn, C. A. Handwerker, J. E. Blendell, W. C. Carter, and A. R. Roosen, "Equilibrium Shape of Internal Cavities in Sapphire", *J. Am. Ceram. Soc.*, **80**[1], 62-8 (1997).
[15] C. A. Powell-Dogan, and A. H. Heuer "Microstructure of 96% Alumina Ceramics: III, Crystallization of High-Calcia Boundary Glasses", *J. Am. Ceram. Soc.*, **73**[12], 3684-91 (1990).
[16] A. G. Evans "Microfracture from Thermal Expansion Anisotropy – I. Single Phase Systems", *Acta Metallurgica*, **26**, 1845-53 (1978).
[17] E. D. Case, J. R. Smyth, and O. Hunter "Grain-Size Dependence of Microcrack Initiation in Brittle Materials", *J. Mat. Sc.*, **15**, 149-53 (1980).
[18] E. D. Case, J. R. Smyth, and O. Hunter, "Microcracking in Large Grain Al_2O_3", *Mater. Sc. Eng.*, **51**, pp. 175-9 (1981).
[19] D-Y Kim, S. M. Wiederhorn, B.J. Hockey, C. A. Handwerker, and J. E. Blendell, "Stability and Surface Energies of Wetted Grain Boundaries in Aluminum Oxide", *J. Am. Ceram. Soc.*, **77**[2] 444-53 (1994).
[20] D. R. Clarke, "On the Equilibrium Thickness of Intergranular Glass Phases in Ceramic Materials", *J. Am. Ceram. Soc.*, **70**[1] 15-22 (1987).
[21] J. E. Blendell, W. C. Carter, and C. A. Handwerker, "Faceting and Wetting Transitions of Anisotropic Interfaces and Grain Boundaries", *J. Am. Ceram. Soc.*, **82**[7] 1889-900 (1999).
[22] H. D. Ackler and Y.-M. Chiang, "Effect of Initial Microstructure on Final Intergranular Phase Distribution in Liquid Phase Sintered Ceramics", *J. Am. Ceram. Soc.*, **82**[1] 183-89 (1999).

Table 1: Effect of grain boundary thickness on residual stresses in alumina

Thickness (nm)	20	60	100	140
Stress Invariant 1 (MPa)	379 to -569	324 to -596	285 to -593	258 to -586
Max. Principal Stress (MPa)	318	271	237	218

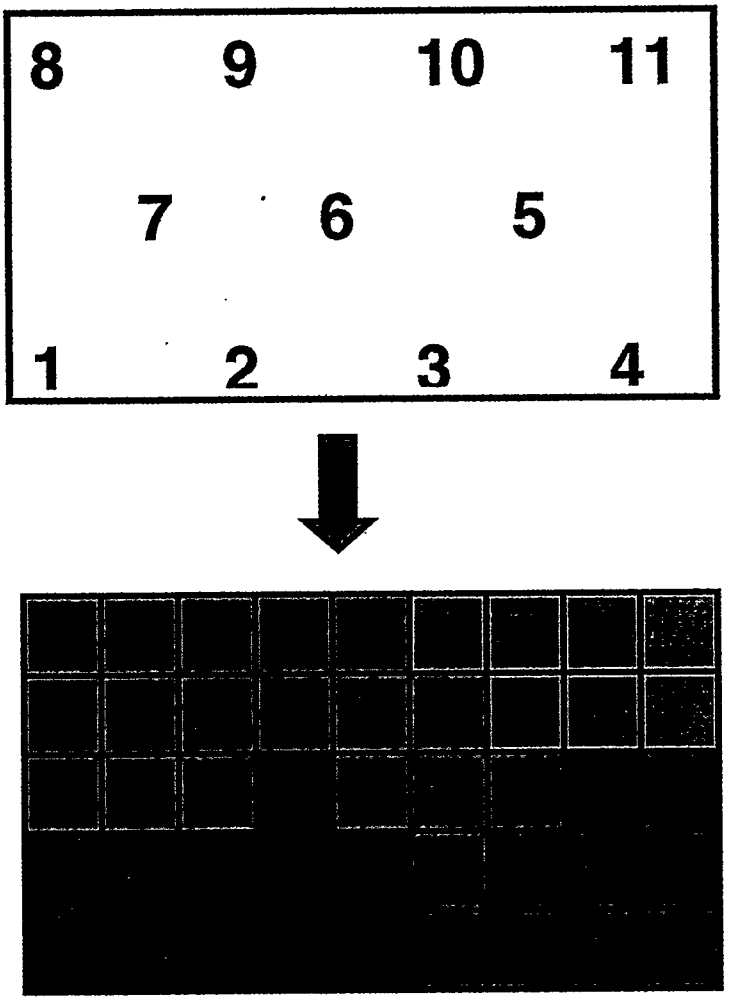

Fig. 1: Transformation of hexagonal grid to a square grid.

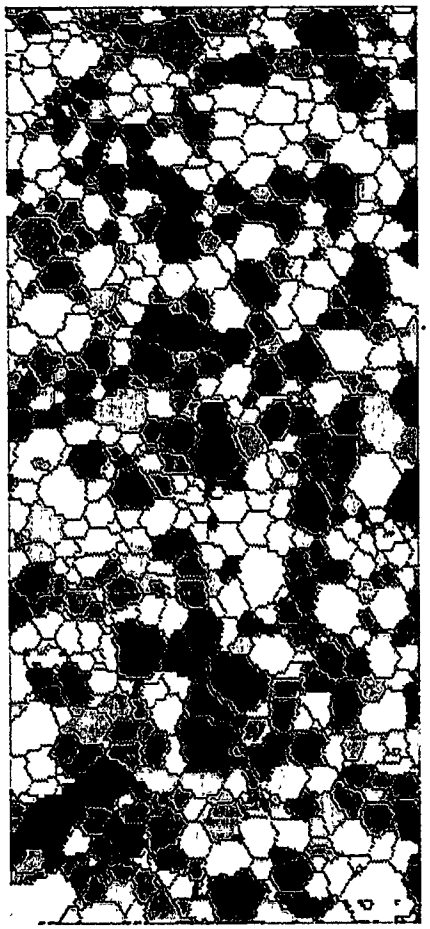

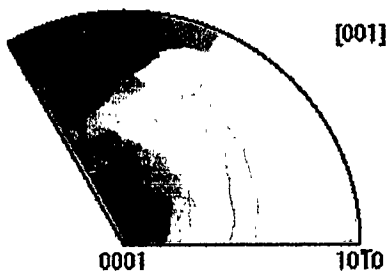

(a)

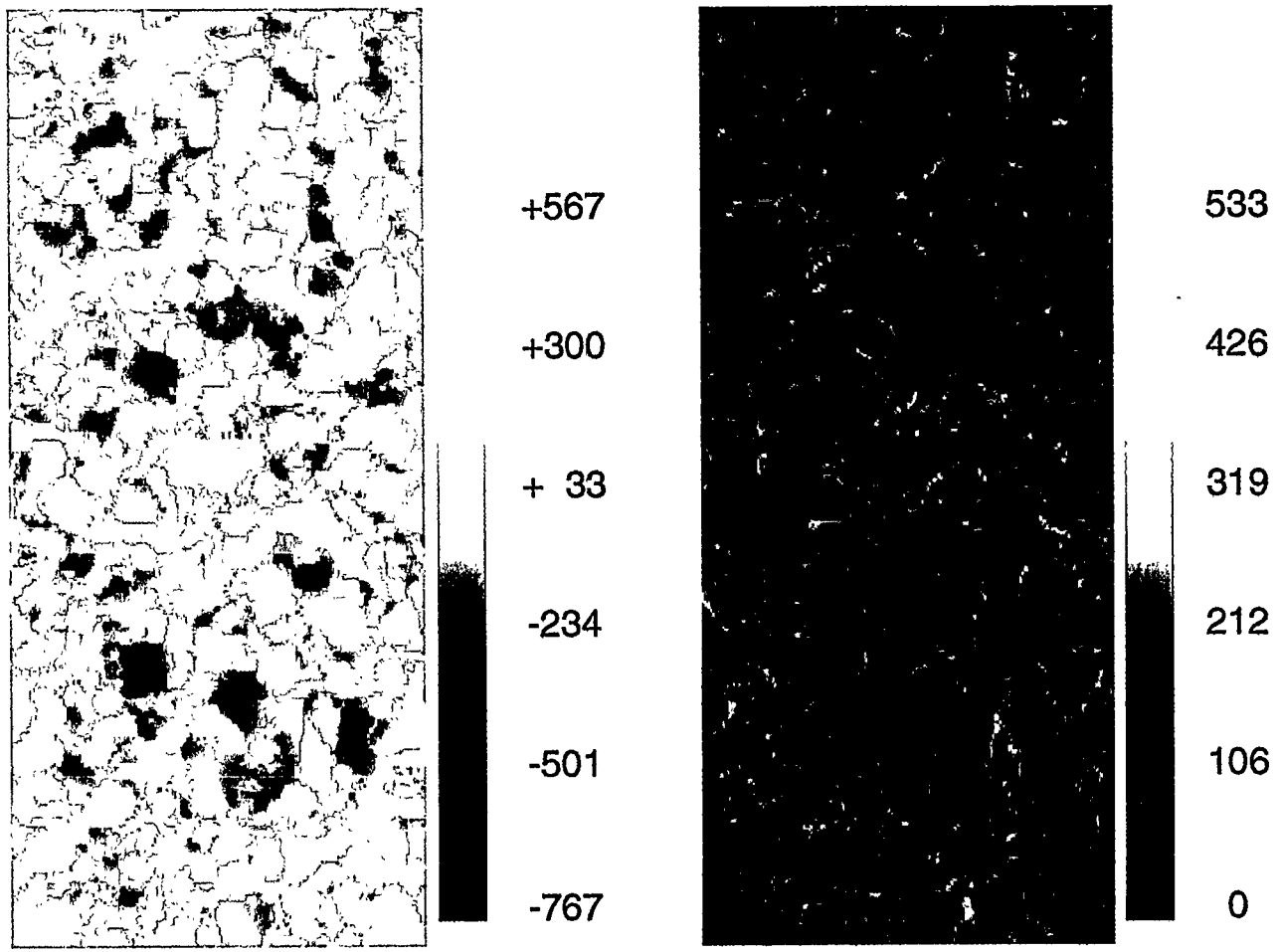

(b) (c)

Fig. 2: Residual stress distribution in untextured alumina when ΔT=-1500°C. (a): Microstructure with grain normals given by the stereographic triangle, (b): Stress Invariant 1 ($\sigma_{11}+\sigma_{22}$) in MPa, and (c): Maximum Principal Stress (σ_{11}) in MPa.

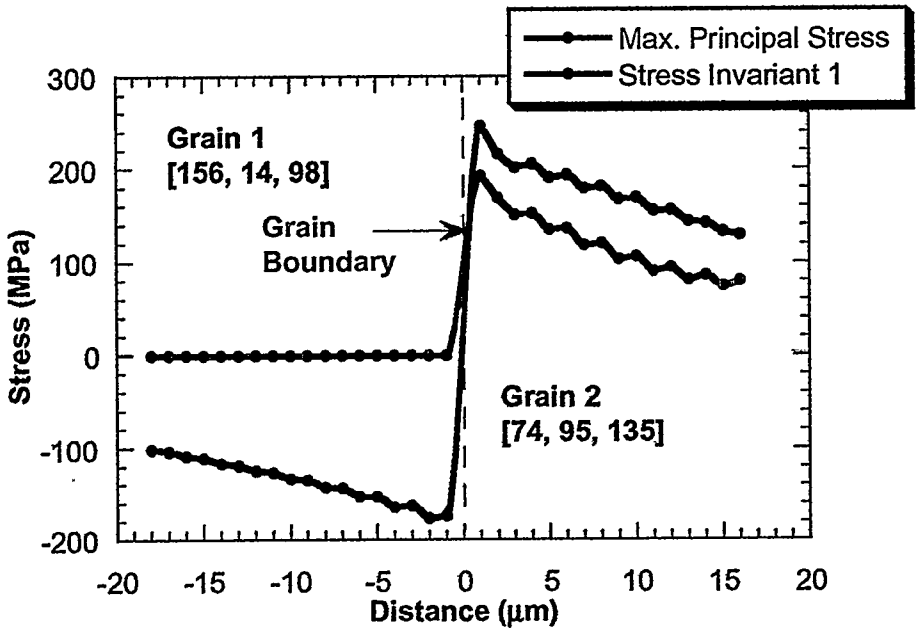

Fig. 3: Residual stress change across a grain boundary

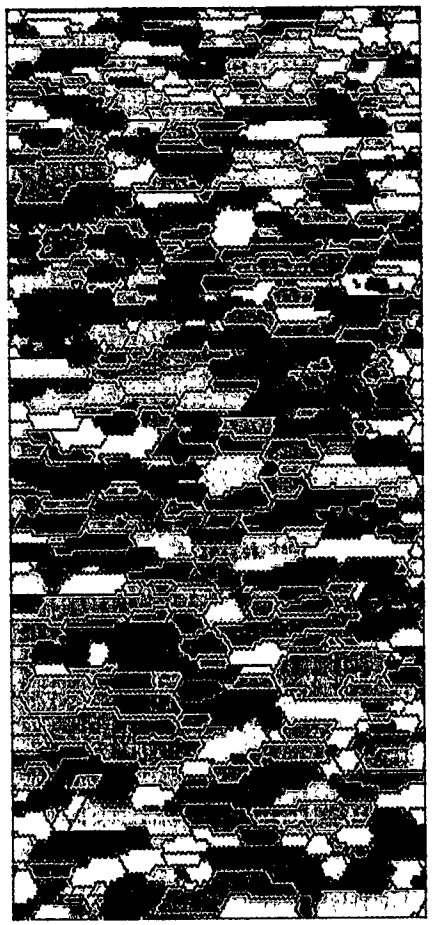

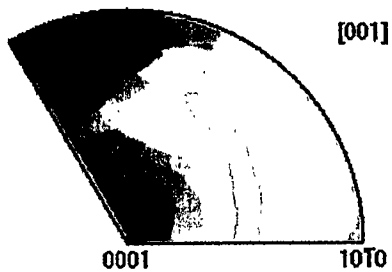

(a)

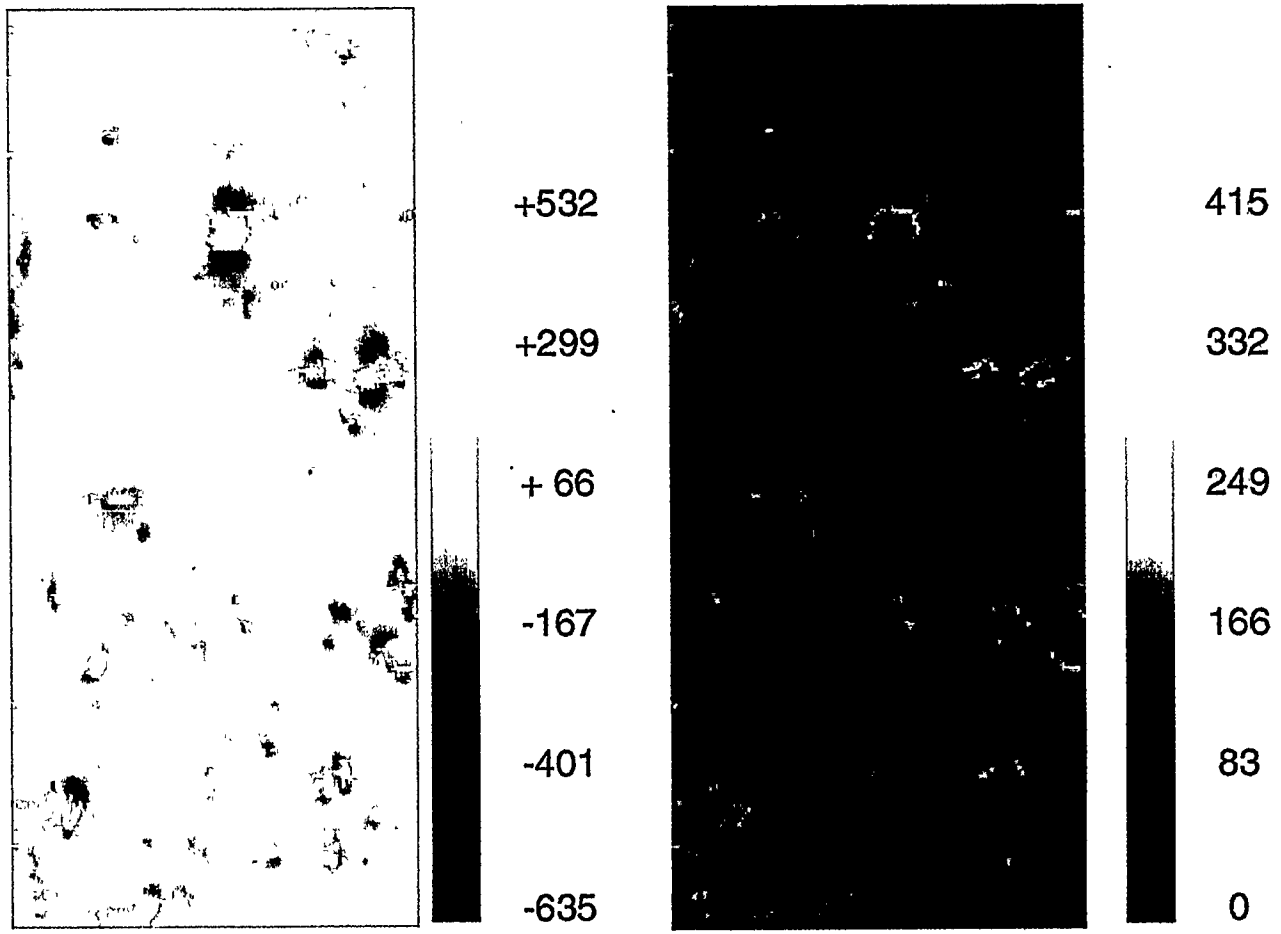

Fig. 4: Residual stress distribution in textured alumina when ΔT=-1500°C. (a): Microstructure with grain normals given by the stereographic triangle, (b): Stress Invariant 1 ($\sigma_{11}+\sigma_{22}$) in MPa, and (c): Maximum Principal Stress (σ_{11}) in MPa.

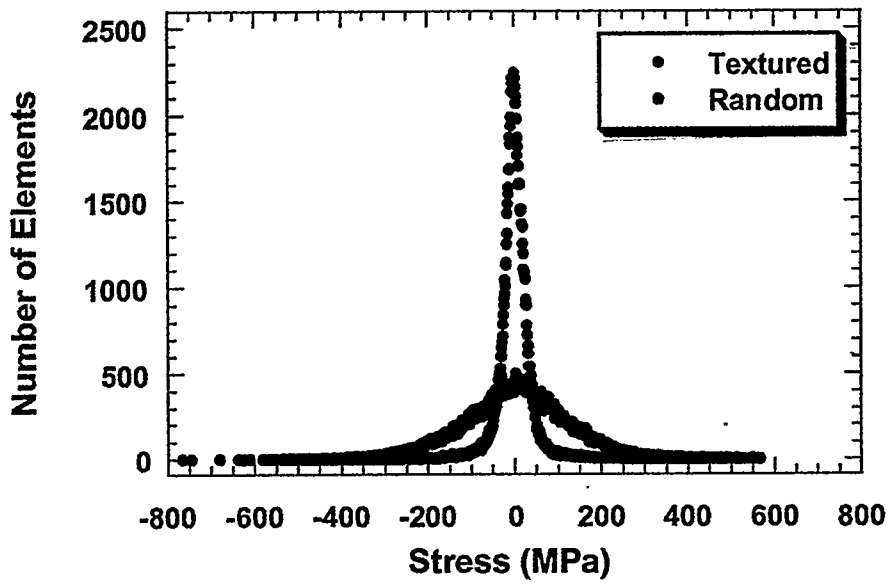

Fig. 5: Residual stress distribution in textured and randomly oriented samples showing Number of elements versus Stress (Stress Invariant 1).

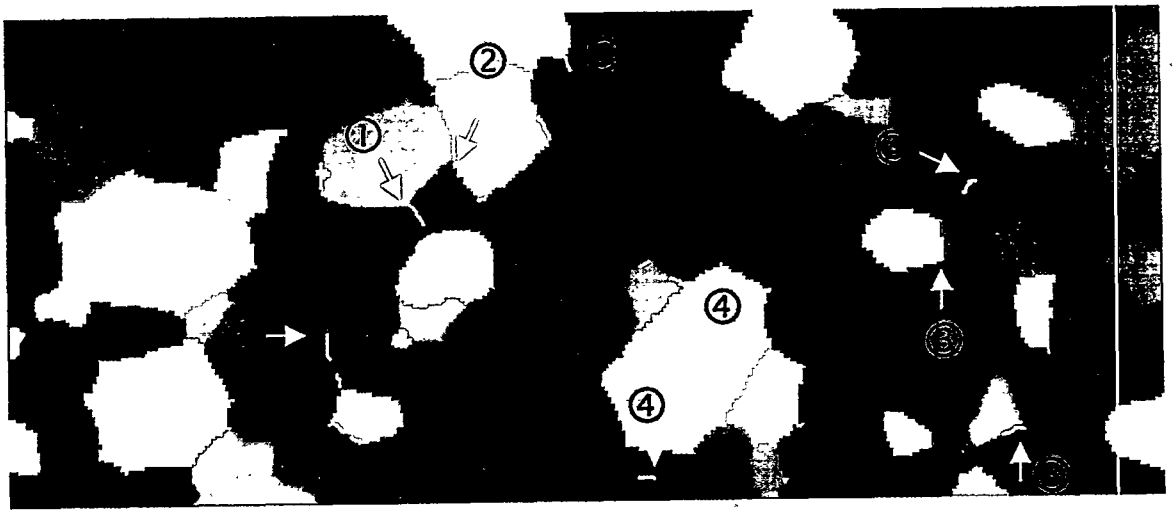

Fig. 6: Microstructure of untextured alumina showing different grains. Numbers indicate microcrack initiation and propagation with increasing temperature difference. ① is -925, ② is -1000, ③ is -1100, and ④ is -1500°C.

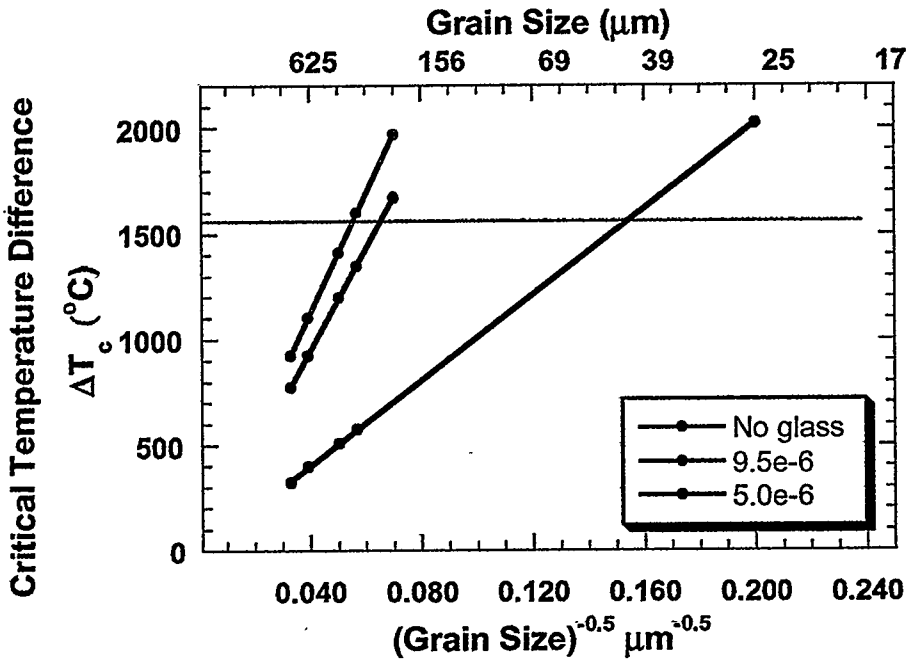

Fig. 7: Critical temperature difference vs. grain size in alumina for no glass and two different grain boundary glass properties (α=9.5x10^{-6} and 5x10^{-6} /°C).

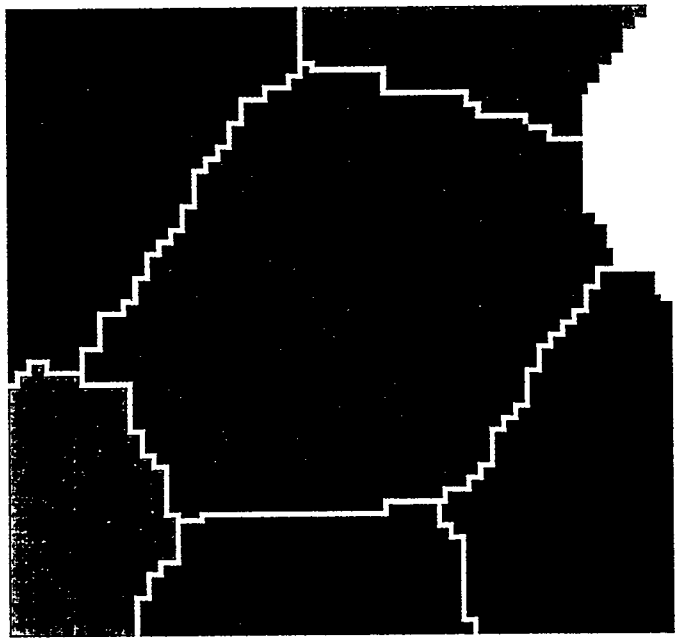

Fig. 8: Microstructure used to evaluate the effect of boundary thickness on residual stresses and microcrack initiation.

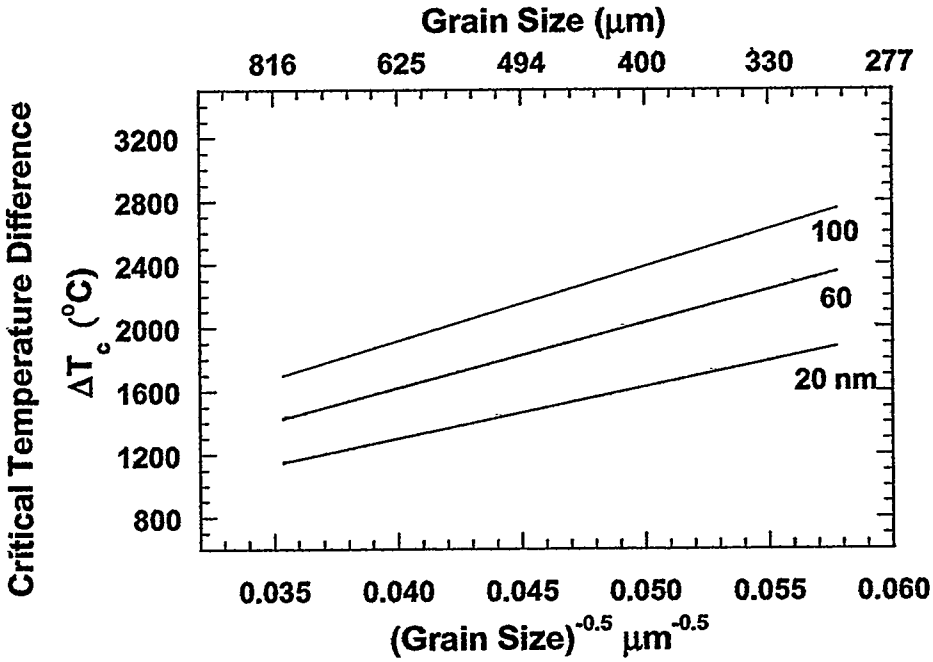

Fig. 9: Effect of grain boundary thickness on critical temperature for cracking.